Annual Temperature and Radiobrightness Signatures for Bare Soils

Yuei-An Liou *Student Member, IEEE* and A. W. England, *Fellow, IEEE*

Abstract— **We have developed physically based, diurnal, and annual models for freezing/thawing moist soils subject to annual insolation, radiant heating, and cooling, and sensible and latent heat exchanges with the atmosphere. Both models have the same weather forcing, numerical scheme, and soil constitutive properties. We find that surface temperature differences over a diurnal cycle between the annual and diurnal models are as much as −5 K in March, −7 K in June, −4 K in September, and 5 K in December for 38% (by volume fraction) moist soil. This difference occurs because the annual model includes the history of energy fluxes at the surface of the soil. The annual model is linked to microwave emission models for predictions of temporal radiobrightness signatures. The model predicts a relatively weak decrease in diurnal differences in soil temperature with increased moisture content, but a significant decrease in diurnal differences in radiobrightness. It also exhibits notable perturbations in radiobrightness when soils freeze and thaw. The moisture dependent, day-to-night radiobrightness difference is enhanced by as much as −42 K at 19.35 GHz horizontal polarization for frozen soil if daytime thawing occurs.**

I. Introduction

LAND surface processes strongly influence the dynamics of the atmosphere over a wide range of space and time scales through exchanges of momentum, moisture, and energy. Soil surface temperature and moisture are key parameters in that they are products of the energy balance between the land and atmosphere. They are also diagnostic parameters in that they govern infrared and microwave emission. Reliably modeling soil surface temperature and moisture are crucial to simulate land-atmosphere interactions and to study radiometric signatures of bare or sparsely vegetated soil.

The focus of this paper is upon the radiobrightness of moist agricultural soils in northern prairie during periods when they are bare of vegetation. Such conditions exist over significant periods of a year for many fields in the northern Great Plains and on the steppes of Asia. None of these fields will fill a resolution cell of a satellite sensor such as the Special Sensor Microwave/Imagers (SSM/I) which have spatial resolutions of 69 × 43 km at 19.35 GHz, 37 × 28 km at 37.0 GHz, and 15 × 13 km at 85.5 GHz [1].

One strategy for synthesizing an expected radiobrightness for a resolution cell would be to aggregate the predicted radiobrightnesses of typical landcover types for the cell according to their expected occurrence throughout an annual cycle. The bare field, or one that is covered by stubble, would be an expected occurrence in agricultural prairie—especially during spring and fall when hydrologists would particularly like to know the quantity of water that is stored in soil or snow. Our overarching objective in this and a companion paper [2] is to develop an expected annual radiobrightness for these bare soils.

Several one-dimensional thermal models have been developed for bare rocks or soils to predict their thermal infrared (TIR) or thermal microwave (radiobrightness) signatures over diurnal periods. Watson [3] applied the Laplace transform method to develop a diurnal model for rock and dry soils. He proposed using diurnal temperature extremes—a measure of a rock's thermal inertia—to discriminate among rock types in TIR images. Kahle [4] developed a diurnal finite difference model for moist soils and proposed using thermal inertia to discriminate among various soils. Price [5], [6] developed a similar model and demonstrated that thermal inertia could be used to infer soil moisture. England [7] developed a diurnal finite element model for freezing and thawing soils to examine the empirical observation that a combination of 10 and 37 GHz radiobrightness from the Scanning Multichannel Microwave Radiometer (SMMR) could be used to map frozen and thawed prairie soils [8], and to extend the TIR-based, thermal inertia technique of estimating soil moisture to the SSM/I's spectral range of 19–85 GHz [9].

None of these diurnal models, nor any of the more recent remote sensing thermal models for vegetation covered terrains, place the diurnal thermal event in an annual context, nor do they incorporate physical models of freezing point depression or of coupled thermal and moisture transport. Using a variable time interval Laplace method to create an annual model for dry soils, Liou and England [10] found significant differences in predicted surface temperatures between the annual model and an equivalent diurnal model. Because soil temperature is a convolution of many past diurnal events, the seasonal history is embedded in the surface temperature. In our companion paper [2], we report on a finite difference, coupled temperature and moisture, diurnal radiobrightness model based upon the thermal modeling approach of de Vries [11] and advanced by Milly and others [12]–[17]. However, this coupled model is too computationally intensive to become a practical annual model.

In this paper, we present the finite element annual thermal/radiobrightness model for moist soils that are subject to freezing and thawing, and compare the model's predictions with those of our equivalent diurnal model [7]. Our specific

Manuscript received September 26, 1995; accepted March 12, 1996. This work was supported by NASA under Grant NAGW-3430.

The authors are with the Department of Electrical Engineering and Computer Science and the Department of Atmospheric, Oceanic, and Space Sciences, University of Michigan, Ann Arbor, MI 48109-2122 USA (e-mail: yueian@eecs.umich.edu) and (e-mail: england@eecs.umich.edu).

Publisher Item Identifier S 0196-2892(96)05142-X.

objectives are to extend our earlier findings for dry soils [10] to the more interesting case of the moist, freezing and thawing soils found in northern prairie; and to identify appropriate lower boundary temperatures by latitude and day-of-year for use as lower boundary temperatures in our coupled model for bare, moist soils [2]. The use of this lower boundary temperature places the coupled diurnal model in the approximate thermal context of an annual model. We also achieve a more rapid convergence of the coupled model by initializing its temperature profile with the temperature profile from this annual model for latitude and day-of-year.

II. Thermal Models

A. Soil Constitutive Properties and Thermal Models

Soil temperatures are obtained by solving the one-dimensional heat flow equation within soil

$$\frac{\partial}{\partial t}(C_p(T_g)\cdot T_g(z,t)) = \frac{\partial}{\partial z}\left(\lambda(T_g)\cdot\frac{\partial T_g(z,t)}{\partial z}\right) \quad (1)$$

where C_p is the apparent volumetric heat capacity of the soil at constant pressure (J/m^3-K), $T_g(z,t)$ is the ground temperature at depth z (m) and time t (s), and λ is the thermal conductivity (W/m-K). Following Andersland et al. [18], the apparent volumetric heat capacity is described by

$$C_p = C_d + C_i(\theta-\theta_u) + C_u\theta_u + L_f\frac{\partial\theta_u}{\partial T} \quad (2)$$

where C_d is the volumetric heat capacity of dry soil matrix, C_i is the volumetric heat capacity of ice, C_u is the volumetric heat capacity of unfrozen water, θ is the total water content, (m^3/m^3), θ_u is the unfrozen water content, and L_f is the volumetric latent heat of fusion (J/m^3). Soil thermal conductivity is computed by using the de Vries' model [11]

$$\lambda = \frac{\sum_{i=1}^{n} k_i\theta_i\lambda_i}{\sum_{i=1}^{n} k_i\theta_i}, \quad (3)$$

where k_i, $i = 1,\cdots,n$ is the weighting function of the ith constituent; θ_i, $i = 1,\cdots,n$ is the volumetric content of the ith constituent; and λ_i, $i = 1,\cdots,n$ is the thermal conductivity of the ith constituent.

Fig. 1 shows the apparent volumetric heat capacity, unfrozen water content and thermal conductivity of 17% and 38% (by volume fraction) moist soils versus temperature. Fig. 1(a) indicates that unfrozen water content decreases exponentially with decreasing temperature below the depressed freezing point (DFP) [18] and the rate of decrease depends upon soil texture. In general, the lower the moisture content, the lower the DFP. The DFP is 267.2 K for 17% moist soil and 272.5 K for 38% moist soils. In this paper, we chose a silt loam because it is typical of prairie soils. Typical silt loams have a porosity, field capacity and wilting point of 48%, 28.6%, and 13.3%, respectively. Their dry substance consists of 19% sand, 22.5% clay, and 58.5% silt [19]. Soil constituents, water, ice, and air have very different thermal properties as shown in Table I. Fig. 1(b) shows that moist soils have an extremely high heat capacity as moisture begins to freeze at temperatures slightly lower than the DFP. Fig. 1(c) shows that soils with a higher moisture content have a higher thermal conductivity below the DFP, while those with a lower moisture content behaves weakly in the opposite sense.

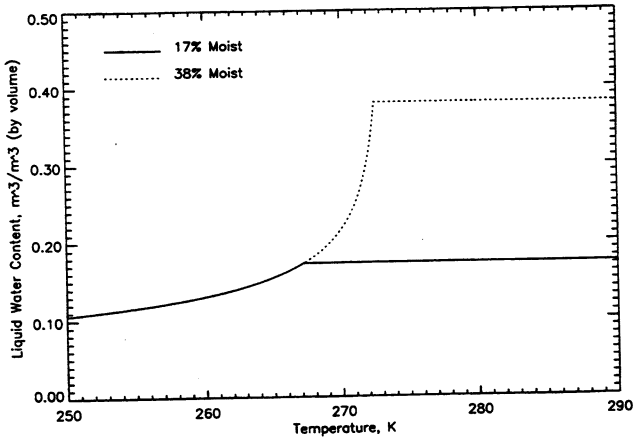

(a)

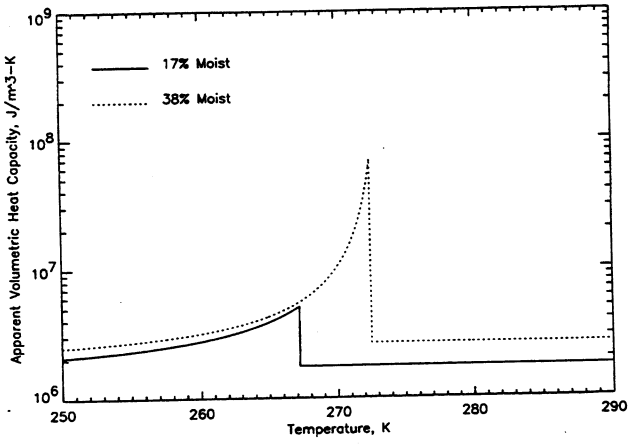

(b)

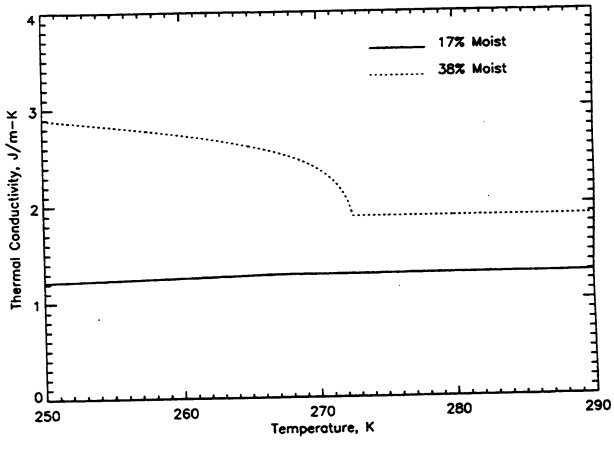

(c)

Fig. 1. (a) Unfrozen water content. (b) Apparent volumetric heat capacity. (c) Thermal conductivity. These soil constitutive properties are applied to both diurnal and annual models.

C_p and λ are an aggregate of the physical properties of all of the soil constituents. Because some of these are temperature

TABLE I
THERMAL CONDUCTIVITIES, VOLUMETRIC HEAT CAPACITIES, AND DENSITIES OF SOME SOIL MATERIALS, WATER, AND AIR AT 10°C AND OF ICE AT 0°C (AFTER DE VRIES [11])

Substance	λ, W/m-K	C, J/m^3-K	ρ, kg/m^3
Quartz	8.892	2.009×10^6	2660
Clay	2.930	1.894×10^6	2650
Water	0.586	4.194×10^6	1000
Ice	2.240	1.937×10^6	917
air	0.249	1.237×10^3	1.231

dependent, the heat flow equation is highly nonlinear with soil temperature. The problem becomes particularly difficult as the state of free water within soil changes and phase boundaries propagate. To solve (1), we used the finite element scheme of England's model [7] which tracks isotherms within the soil.

The term in parenthesis on the right of (1) is the negative of the energy flux at depth z and time t. Equation (1) is solved by imposing the following boundary conditions of weather forcing at the land-atmosphere interface and a zero energy flux at a depth beyond the annual thermal pulses.

B. Boundary Conditions

The energy budget at the land-atmosphere interface is a balance among radiant heat, sensible heat, and latent heat. The energy flux available to soil at the surface is

$$F(0,t) = F_{\text{sun}}(t) + F_{\text{sky}}(t) - F_{\text{sh}}(t) - F_{\text{lh}}(t) - F_g(t) \quad (4)$$

where F_{sun} is insolation reduced by cloud extinction, atmospheric absorption, albedo, and the cosine of the zenith angle; F_{sky} is sky brightness with a correction for cloud cover; F_{sh} is the sensible heat transfer from the land to the atmosphere; F_{lh} is the latent heat transfer from the land to the atmosphere; and F_g is gray-body emission from the soil's surface. F_{sun}, F_{sky} and F_g have been further described in England [7]. The sensible heat transfer from the bulk transfer method may be expressed by [20]

$$F_{\text{sh}} = \rho_a \cdot c_{p,a} \cdot \left(\frac{T_g(0,t) - T_a(z_r,t)}{r_a} \right) \quad (5)$$

where r_a is the aerodynamic resistance (s/m), ρ_a is the air density (kg/m^3), $c_{p,a}$ is the air specific heat at constant pressure (J/kg-K), $T_a(z_r,t)$ is the air temperature at a reference height z_r and time t (K). The latent heat transfer is given by [21]

$$F_{\text{lh}} = f \cdot \frac{F_{\text{sh}}}{B} \quad (6)$$

where f is evaporation efficiency, and B is the Bowen ratio. The evaporation efficiency, a ratio between real evaporation and potential evaporation, is chosen to be a linear function of soil moisture content with values between 0 and 1 corresponding to wilting point and saturation, respectively.

The Bowen ratio may be estimated by [21]

$$B = \gamma \cdot \frac{T_a(0,t) - T_a(z_r,t)}{e(0,t) - e(z_r,t)} \quad (7)$$

where γ is the psychometric constant (Pa/K), $e(0,t)$ is surface water vapor pressure (Pa), and $e(z_r,t)$ is air vapor pressure at the reference height (Pa). Air temperature is assumed to be the climatic value for the time-of-day and day-of-year of the location for which the model was run. For our purposes, this location was chosen to be Sioux Falls, SD. The partial pressure of the water vapor was arbitrarily chosen to be constant through a day and of a value that would yield a 40% humidity at solar noon. The psychometric constant is expressed as [21]

$$\gamma = \frac{c_{p,a} \cdot p}{0.622 \cdot L_e} \quad (8)$$

where p is the atmospheric pressure at the boundary layer (Pa), and L_e is the latent heat of evaporation of water (J/kg).

The saturation water vapor pressure is obtained by solving

$$\log(0.01e) = 9.4041 - \frac{2354}{T} \quad (9)$$

where log is decimal logarithm, and T is the temperature. Equation (9) is from the Clausius-Clapeyron equation with higher-order terms neglected [22].

C. Model Results

The ground warms quickly as the sun rises. Capturing these rapid changes with the numerical integrations requires time intervals of 10 min or less. Because there are over fifty thousand 10-min intervals in an annual cycle, compared to only 144 intervals in a diurnal cycle, the numerical simulation of the annual model becomes computationally intensive. To gain quicker convergence, the annual equilibrium temperature (AET) is assigned as the initial temperature of soil at all depths and all time-steps. The AET is chosen so that the sum of incoming insolation and sky radiation and the outgoing emission from the surface are in balance. A similar treatment for the initial temperature is applied to the diurnal model.

The annual temperature at all depths and all time-steps generally differs from AET by less than 40 K so that its profile can be sufficiently described by 40 dynamic one-K isotherms. Similarly, 20 one-K isotherms are generally sufficient for a diurnal model. The actual number of isotherms is not only dependent upon time scale, but also dependent upon moisture content and state.

Fig. 2 shows the surface temperatures for 17% moist soil with latent heat transfer, and 38% moist soil with and without latent heat transfer for March, June, September, and December at a northern latitude of 43.5 degrees (that of Sioux Falls, SD). Soils appear to resist changes in temperature as moisture freezes and thaws (Fig. 2 for dates 03/22 and 12/22). A comparison of Fig. 2(a) and (b) shows 17% moist soils respond to the weather forcing at the land-atmosphere interface faster and to a greater extent than to the 38% moist soils, i.e., wetter soils have a higher apparent thermal inertia. The difference in the diurnal variation is 7.8 K for March, 6.8 K for June, 5.4 K for September, and 5.2 K for December. A comparison between Fig. 2(b) and (c) shows that latent heat exchanges with the atmosphere tend to suppress diurnal temperature variation. These decreases are 1 K for March, 4.4 K for June, 2.8 K for September, and 0.01 K for December. The decreases are in the direction to enhance the effect of moisture on apparent thermal inertia.

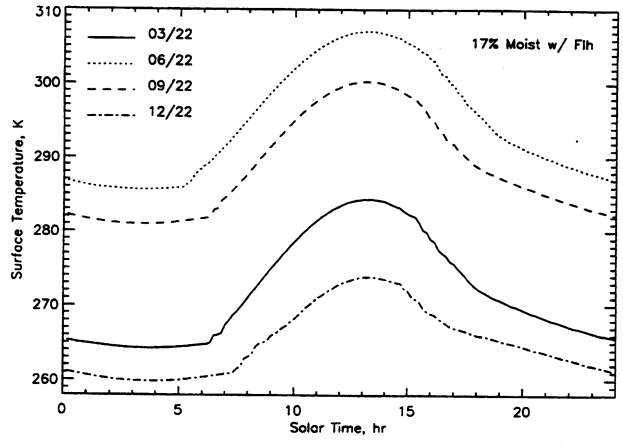

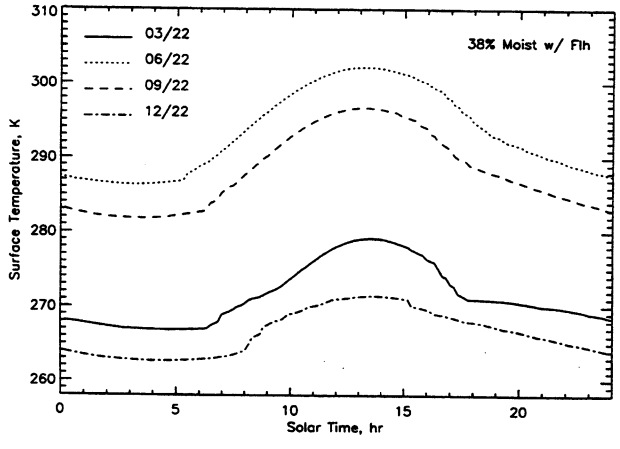

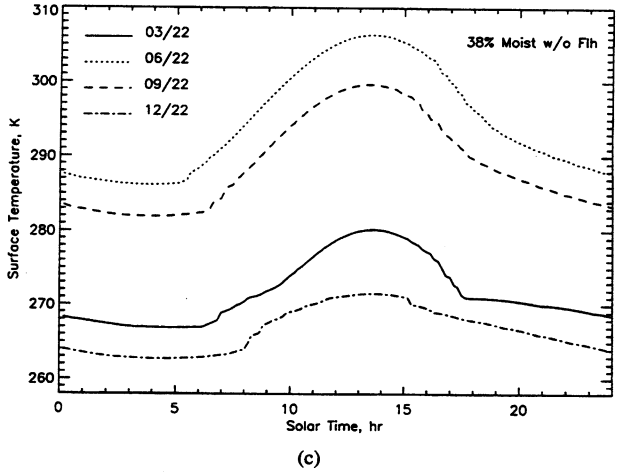

Fig. 2. Diurnal surface temperatures for: (a) 17% with latent heat transfer; (b) 38% moist soils with latent heat transfer; and (c) 38% moist soils without latent heat transfer for 03/22, 06/22, 09/22, and 12/22.

The thermal conductivity of 38% moist soil is more than two times larger than that of 17% moist soil at temperatures below the DFP so that the apparent thermal inertia is greater in March and December for more moist soils [Fig. 1 (c)]. More importantly, apparent volumetric heat capacity of 38% moist soil is more than an order of magnitude greater than

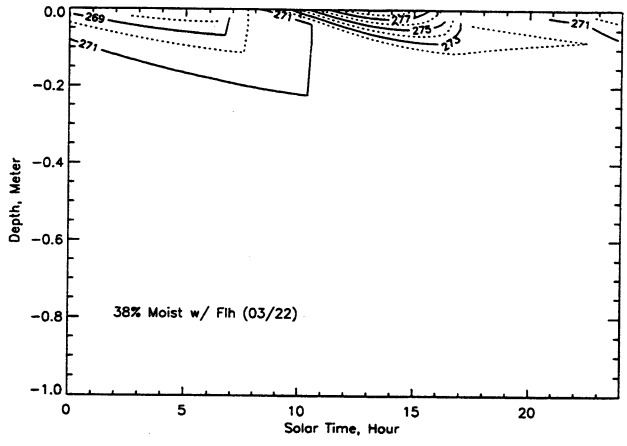

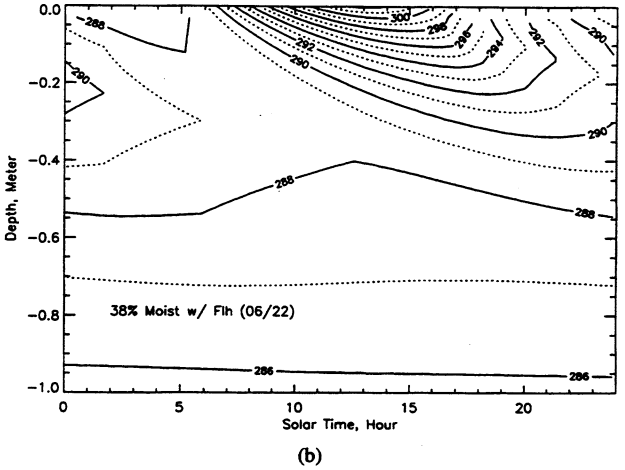

Fig. 3. 38% moist soil isotherms with latent heat transfer for 03/22 and 06/22.

that of 17% moist soil at temperatures between their DFP's [Fig. 1(b)].

Fig. 3 shows the diurnal isotherms for 38% moist soil with latent heat transfer for March and June. Notable characteristics include: 1) isotherms are created after sunrise and start to merge some time after peak insolation; 2) temperature gradients in the first few centimeters are much larger during the day than during the night; 3) soil temperatures at depths below 0.8 meter remain approximately constant during a diurnal cycle; and 4) diurnal thermal pulses penetrate approximately 50 cm in June but less than 20 cm in March when a large fraction of the insolation is used to melt water. We present only March and June isotherms because December isotherms are like those in March, and September isotherms are like those in June.

Fig. 4 shows the diurnal isotherms for 17% moist soil with latent heat transfer for March and June. Two major differences between Figs. 3 and 4 are: 1) there are more one-K isotherms for 17% moist soil than there are for 38% moist soil; and 2) penetration depths of thermal pulses in winter are nearly 60 cm for 17% moist soil, but only 20 cm for 38% moist soil. Soil with 17% moisture content is considered relatively dry and has a small amount of free water to freeze or thaw.

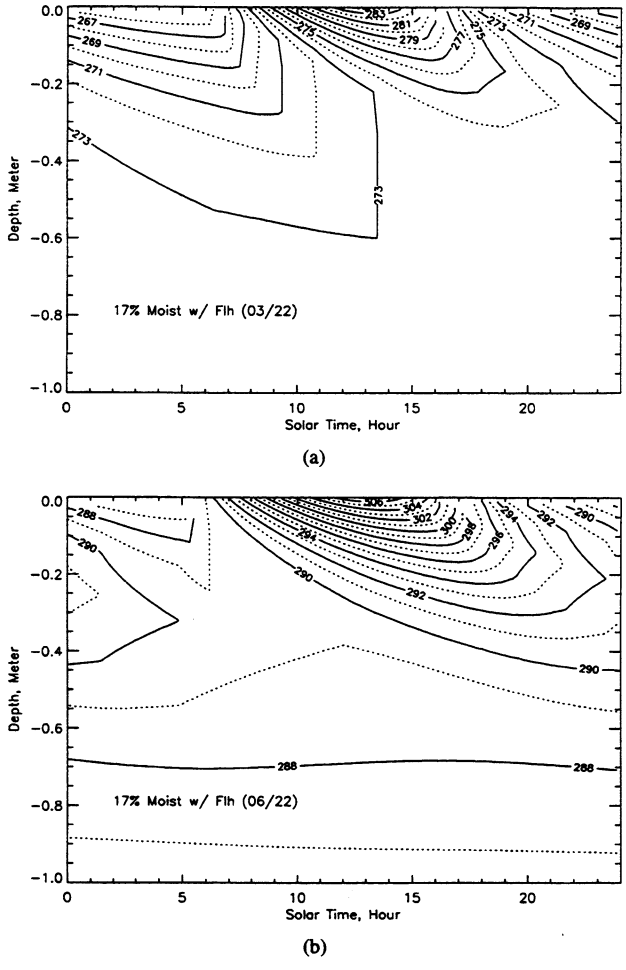

Fig. 4. 17% moist soil isotherms with latent heat transfer for 03/22 and 06/22.

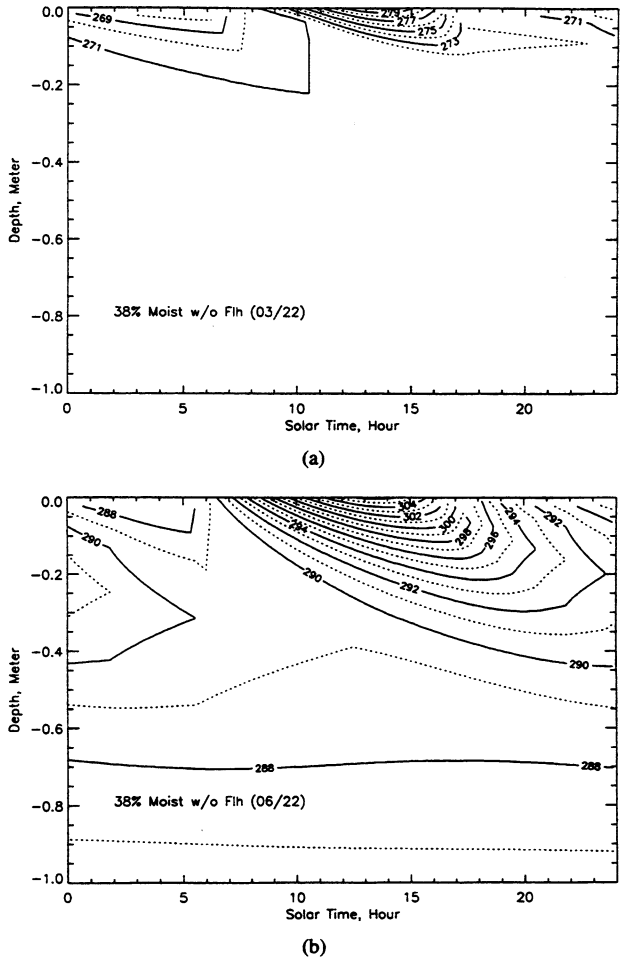

Fig. 5. 38% moist soil isotherms without latent heat transfer for 03/22 and 06/22.

Fig. 5 shows the diurnal isotherms for 38% moist soil without latent heat transfer for March and June. A comparison between Figs. 3 and 5 for March shows that the contours for the no latent heat case and for the latent heat case are nearly the same. Latent heat transfer is essentially turned off when the ground is frozen. For June, the latent heat case has fewer one-K isotherms than the no latent heat case because latent heat transfer reduces the change in soil temperature.

The differences in surface temperatures over a diurnal cycle between annual and diurnal models for 17% and 38% moist soils with latent heat transfer for March, June, September and December are shown in Fig. 6. The range of the differences increases with increasing moisture content—from −3.5 to 2.8 K for 17% moist soil and from −6.6 to 4.8 K for 38% moist soil. This occurs because the drier soil with a lower thermal inertia is more easily modified by current weather forcing and is less dependent upon historical weather forcing.

Latent heat transfer is relatively more important when soils are unfrozen. For September, latent heat transfer and prior summer heating are opposing effects so that the differences between the two models are near zero during nighttime, and only slightly negative during daytime. For June, latent heat transfer and winter cooling contribute in the same sense so that the differences between the two models are about 3 K.

Fig. 7 shows the annual surface temperature variations at four times: 2 am, 6 am, 2 pm, and 6 pm for 17% and 38% moist soils. The differences between the maximum and minimum surface temperatures over an annual cycle for 17 and 38% moist soils are listed in Table II. The differences are larger for 17% moist soil than for 38% moist soil at the four times by about 2 K. This indicates that annual extremes in soil temperature are weakly dependent upon moisture content. However, the annual model predicts significant perturbations in soil temperature with moisture content during the periods of spring thawing and winter freezing as noted in [10]. These perturbations are exaggerated in the temporal radiobrightness signature because of microwave emissivity's dependence upon moisture content and state.

III. Radiobrightness Model

A. Soil Dielectric Properties and Radiobrightness Model

Dielectric properties together with temperature and moisture content/state determine radiobrightness of soil. At temperatures above DFP, we estimate these dielectric properties with

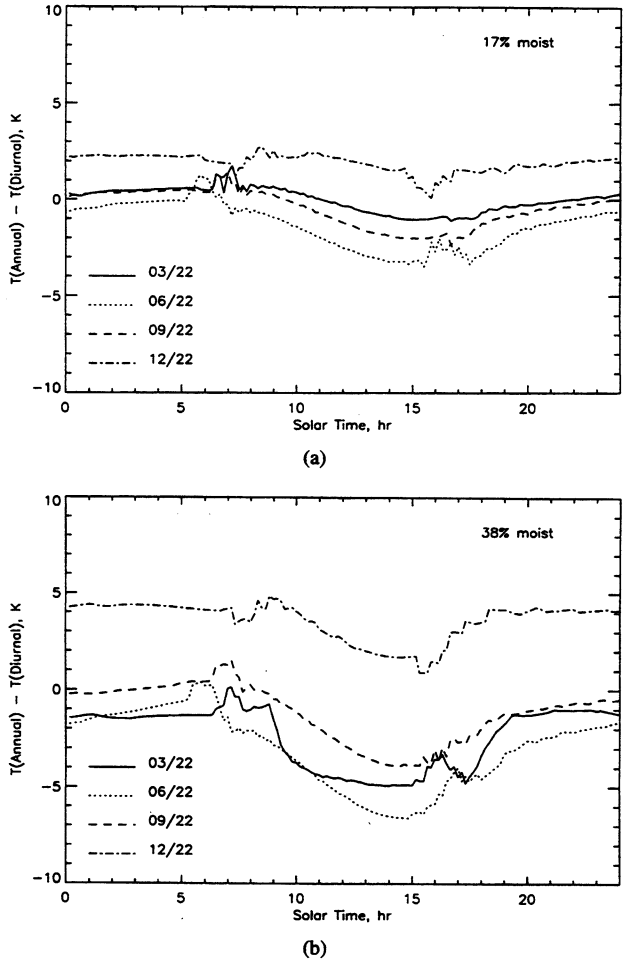

Fig. 6. Differences in diurnal surface temperatures between annual and diurnal models for (a) 17% moist soil and (b) 38% moist soil for 03/22, 06/22, 09/22, and 12/22.

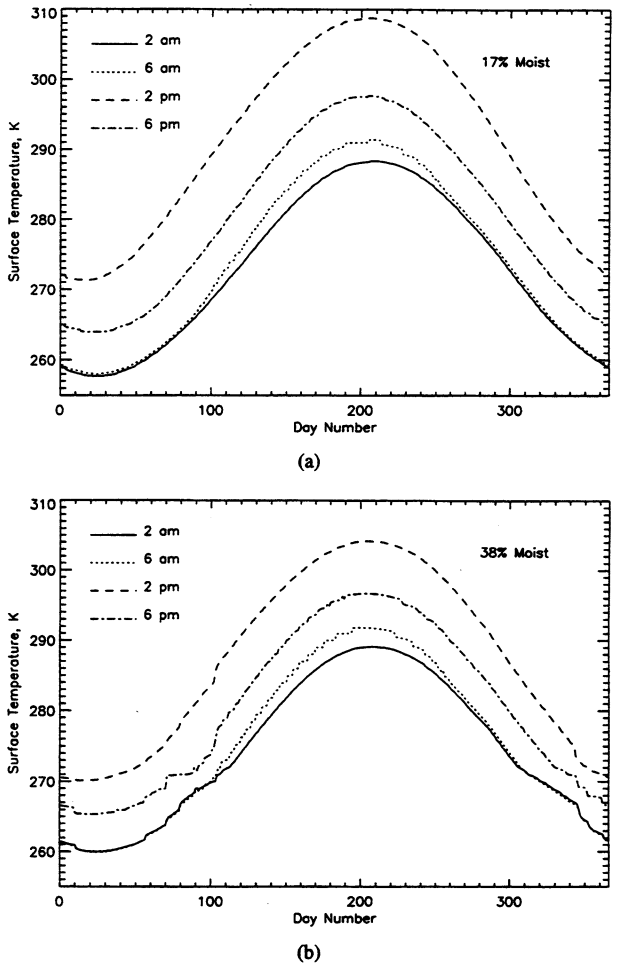

Fig. 7. Annual surface temperature variations at four times: 2 am, 6 am, 2 pm, and 6 p.m. for (a) 17% moist soil and (b) 38% moist soil.

a four-component mixture model of soil solids, air, free water, and bound water [23], [24]. Below DFP, we include the ice component, i.e.,

$$\epsilon^{\alpha} = \theta_s \epsilon_s^{\alpha} + \theta_a \epsilon_a^{\alpha} + \theta_{\mathrm{fw}} \epsilon_{\mathrm{fw}}^{\alpha} + \theta_{\mathrm{bw}} \epsilon_{\mathrm{bw}}^{\alpha} + \theta_i \epsilon_i^{\alpha} \qquad (10)$$

where ϵ is the complex dielectric constant of the soil-water system, α is a constant shape factor, θ denotes the volumetric fraction (m^3/m^3), and the subscripts s, a, fw, bw, and i stand for soil solids, air, free water in the liquid water state, bound water, and ice, respectively. $\alpha, \epsilon_s, \theta_{\mathrm{bw}}$, and ϵ_{bw} are described in Table III. The dielectric constants of free water and ice are described by the Debye equation [24]

$$\epsilon_{\mathrm{fw}/i}^{*} = \epsilon_{w\infty/i\infty}^{*} + \frac{\epsilon_{w0/i0}^{*} - \epsilon_{w\infty/i\infty}^{*}}{1 + j2\pi f \tau_{w/i}} \qquad (11)$$

where $\epsilon_{w0/i0}^{*}$ is the static dielectric constant of liquid water or ice, $\epsilon_{w\infty/i\infty}^{*}$ is the high frequency limit of $\epsilon_{\mathrm{fw}/i}^{*}, \tau_{w/i}$ is the relaxation time of liquid water or ice(s), and f is the frequency, Hz.

Fig. 8 shows the dielectric constants for 17% and 38% moist soils at 19.35, 37, and 85.5 GHz. The magnitudes of both real and imaginary parts of the dielectric constants of liquid water and, thus, of moist soil decrease with increasing frequency. Below DFP, the magnitudes of both real and imaginary parts of the dielectric constants follow the liquid water content and decrease with decreasing temperature.

TABLE II
THE DIFFERENCES BETWEEN THE MAXIMUM AND MINIMUM SURFACE TEMPERATURES OVER AN ANNUAL CYCLE AT FOUR TIMES FOR 17% AND 38% MOIST SOILS

	17%	38%
2 a.m.	30.7	29.1
6 a.m.	33.6	31.9
2 p.m.	37.5	34.1
6 p.m.	33.8	31.3

Wet soils are sufficiently absorptive in the microwave region so that effective emission depths are usually less than a few tenths of a centimeter. This permits a first-order approximation to the radiobrightnesses of bare, quasispecular, wet soils [7], [10].

$$T_b(t) = e \cdot T_{\mathrm{eff}}(t) \qquad (12)$$

where $e = 1 - \Gamma$ is the emissivity of the soil. Γ, the reflectivity

TABLE III
PARAMETERS REQUIRED FOR COMPUTING RADIOMETRIC PROPERTIES OF THE SOIL-WATER SYSTEM

α	0.65 [a]
ϵ_s	$(1.01 + 0.00044\rho_s)^2 - 0.062$ [a]
θ_{bw}	$10 \times dA\rho_b$ [a]
ϵ_{bw}	$31 + j15$ [a]
ρ_s	2658.9 kg/m^3 (soil density) [b]
ρ_b	1382.6 kg/m^3 (bulk density) [b]
d	3 Å (thickness of bound water layer) [a]
A	84000 m^2/kg (soil specific surface) [c]

[a] After [23].
[b] Estimates are based upon the values suggested by [11].
[c] After [18]. It is so chosen to be consistent with themodel for computing liquid water content below DFP.

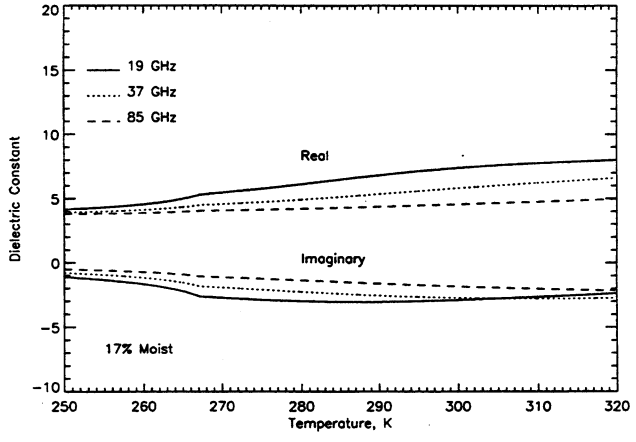

(a)

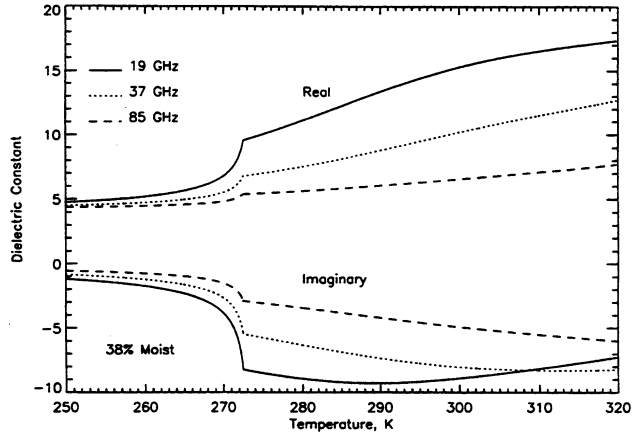

(b)

Fig. 8. Dielectric constants of (a) 17% moist soil and (b) 38% moist soil at 19, 37, and 85 GHz.

of the ground at the land-air interface, is

$$\Gamma = \begin{cases} \left|\frac{\eta_a \cos\theta_a - \eta_g \cos\theta_g}{\eta_a \cos\theta_a + \eta_g \cos\theta_g}\right|^2 & \text{horizontal polarization} \\ \left|\frac{\eta_g \cos\theta_a - \eta_a \cos\theta_g}{\eta_g \cos\theta_a + \eta_a \cos\theta_g}\right|^2 & \text{vertical polarization} \end{cases}$$

where $\eta_g(\eta_a)$ is the intrinsic impedance of the ground (air), θ_a is the incidence angle, and θ_g is the transmission angle. The assumption of a quasispecular soil surface may be adequate at 19.35 GHz—the lowest of the SSM/I frequencies, but it becomes questionable at the higher SSM/I frequencies.

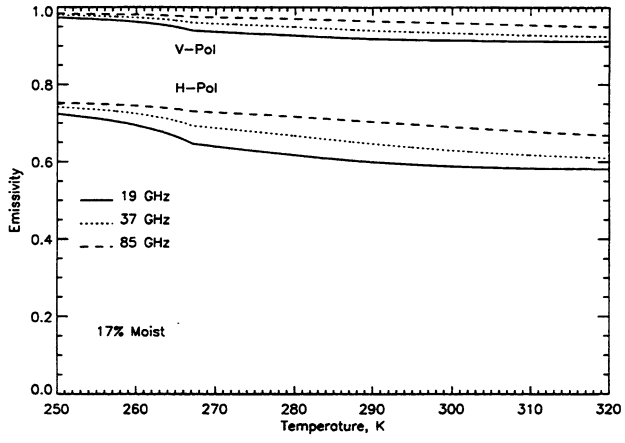

(a)

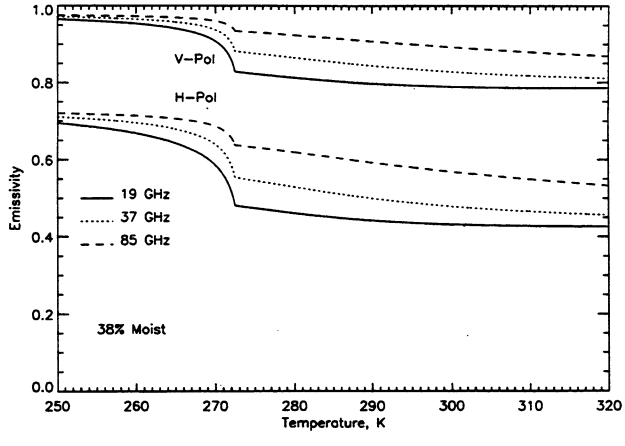

(b)

Fig. 9. Emissivity versus temperature at the 53° angle of incidence of the SSM/I for (a) 17% moist soil and (b) 38% moist soil.

Surfaces look increasingly "black" as they become rough so that we expect the observed radiobrightness of moist soil to be somewhat higher at 37.0 GHz and 85.5 than (12) would predict. This rough-surface correction is beyond the scope of this paper.

The effective ground temperature, T_{eff}, is

$$T_{\text{eff}}(t) = T_g(0,t) + \frac{1}{\kappa_e \sec\theta_g} \cdot \left(\frac{\partial T_g(z)}{\partial z}\right)_{z=0} \tag{13}$$

where κ_e in the first-order correction to surface temperature is the extinction in soil.

The magnitude of extinction for temperatures between 250 K and 320 K at SSM/I frequencies lies between 200 to 1700 for 17% moist soil, and between 200 to 3600 for 38% moist soil. Scattering is ignored because absorption dominates at temperatures above the DFP. At temperatures slightly below the DFP, scatter darkening might still be ignored because liquid water content continues to be significant. At temperatures sufficiently below the DFP, scatter darkening will become important [8].

B. Model Results

Emissivities at 19, 37, and 85 GHz for 17 and 38% moist soils are shown in Fig. 9. Their magnitudes for both

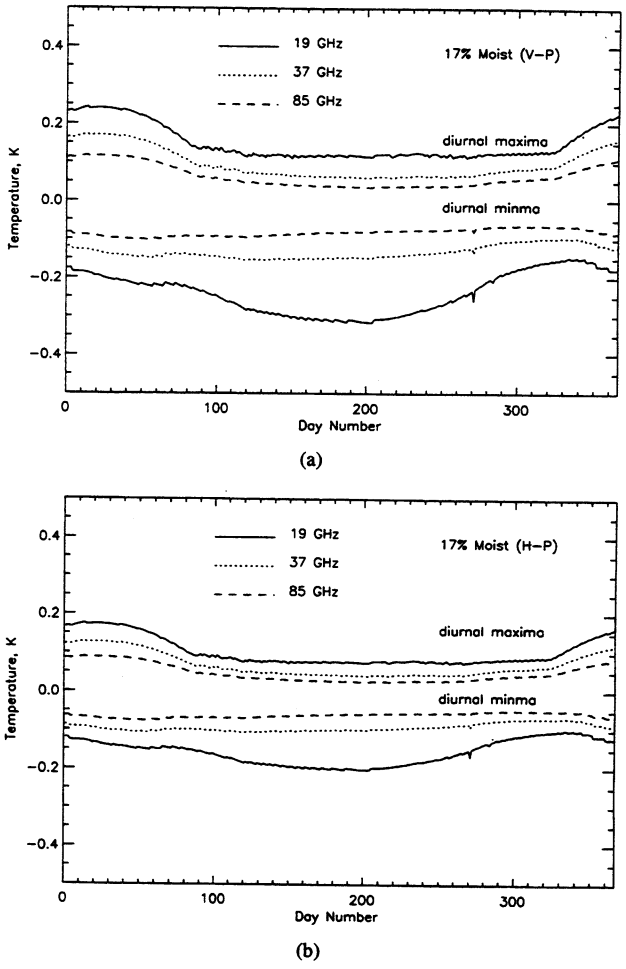

Fig. 10. Diurnal maxima and minima of the first-order terms for (a) vertical polarization and (b) horizontal polarization for 17% moist soil.

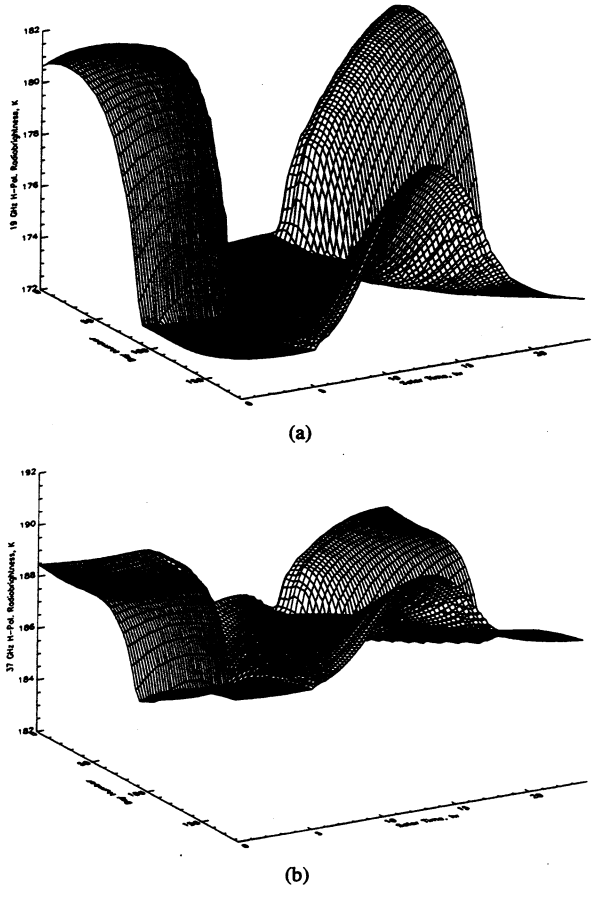

Fig. 11. Semiannual radiobrightness signatures for (a) 19 GHz horizontal polarization and (b) 37 GHz horizontal polarization for 17% moist soil.

polarizations decrease slightly with increasing temperature. The 53° incidence angle is below the range of Brewster angles for 17% moist soil—63° to 71°, or for 38% moist soil—65° to 77°. The strong dependence of emissivity upon liquid water content is apparent in the differences between Fig. 9(a) and (b). These exceed 0.15 at temperatures above DFP, but are less than 0.05 at temperatures a few degrees below DFP.

The diurnal maxima and minima of the first-order terms $(\frac{1}{\kappa_e \sec\theta_t} \cdot (\frac{\partial T_g(z)}{\partial z})_{z=0})$ for 19 GHz vertical and horizontal polarization for 17% moist soil are shown in Fig. 10. They range from −0.32 to 0.24 K for 19 GHz vertical polarization, and from −0.20 to 0.18 K for 19 GHz horizontal polarization. The temporal signatures for the diurnal maxima and minima of first-order terms for 37 GHz and 85 GHz are similar to those of 19 GHz, but with a smaller variation—from −0.16 to 0.17 K for 37 GHz vertical polarization, from −0.11 to 0.13 K for 37 GHz horizontal polarization, from −0.10 to 0.12 K for 85 GHz vertical polarization, and from −0.08 to 0.09 K for 85 GHz horizontal polarization. As soil moisture content increases, the first-order terms become even less important.

Fig. 11 shows semiannual radiobrightness signatures for 19 GHz and 37 GHz horizontal polarization for 17% moist soil. In winter, nighttime radiobrightness corresponds to frozen (effectively dry) soil while daytime radiobrightness reflects melting (in the absence of vegetation and snow). Daytime decreases in radiobrightness are a response to increases in liquid water content.

In spring after soils are completely thawed, radiobrightnesses are nearly linear with temperature except for a small, second-order effect caused by emissivity's dependence upon temperature (Fig. 9). An exponential decrease in radiobrightness occurs at the daytime in early winter. We only show semiannual results because the radiobrightness signatures for the second half year approximately mirror the first half year. The 85 GHz results are not shown because they are similar to but smaller in amplitude than the 19 and 37 GHz results. Results for vertical polarization are not shown for the same reason.

Fig. 12 shows semiannual radiobrightness signatures for 19 and 37 GHz horizontal polarization for 38% moist soil. A comparison between Figs. 11 and 12 demonstrates that 17% and 38% moist soil have extremely different radiobrightness signatures during winter and spring when diurnal freezing and thawing have a more dramatic effect upon more moist soils. During winter or early spring, the day-to-night change in radiobrightness for 38% moist soil could exceed 18 K at 19 GHz, and 9 K at 37 GHz. These variations are more than double those for 17% moist soil. The maximum variations for 38% moist soil occur in late February when soil is thawed

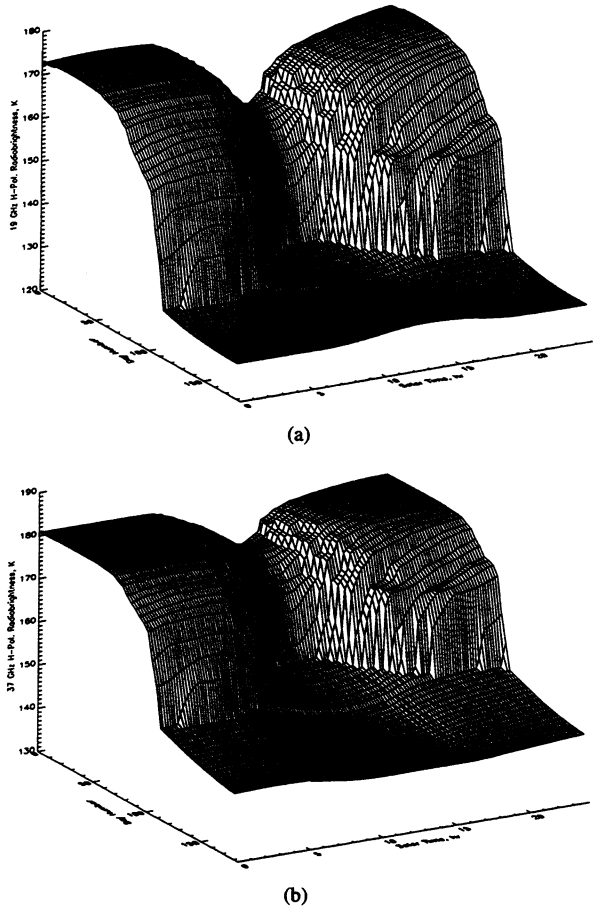

Fig. 12. Semiannual radiobrightness signatures for (a) 19 GHz horizontal polarization and (b) 37 GHz horizontal polarization for 38% moist soil.

during the daytime, but partially frozen at night. Fig. 12 also shows that the day-to-night difference in 19 GHz horizontal radiobrightness is weakly positive in late spring by as much as 3 K, but that the equivalent 37 GHz difference is weakly negative by about −2 K. The contrast is caused by differing soil dielectric behavior with temperature at the two frequencies (Fig. 8).

IV. Discussion

The predictions of this annual radiobrightness model should be compared with relevant data. The model in such a test would be forced by actual weather rather than by expected climate as we have done. As noted in the introduction, a comparison with satellite data (e.g., with data from the SSM/I), is difficult because of the low spatial resolution of these sensors. While there have been diurnal ground observations of bare soil that show the features of our diurnal model (e.g., Wegmüller et al. [25]), there have been no seasonal or annual experiments. Our group has conducted a series of Radiobrightness Energy Balance Experiments in grassland prairie (REBEX-1 [26]) and in wet acidic tundra (REBEX-3 [27]), but have not yet examined the seasonal temperature and radiobrightness signatures of bare moist soil. We do plan such an experiment for the summer of 1996.

While we do not have the desired experimental verification, the annual model reported here indicates that diurnal predictions of land-atmosphere thermal and moisture exchanges should be set in an annual context, that the history of energy exchanges at the land-atmosphere interface has an increasing influence upon soil surface temperatures as moisture content increases, and that the strong moisture dependence of the diurnal extremes in surface temperature predicted by our diurnal model persists in an annual context. The last conclusion will be moderated in the companion paper. Coupling heat and moisture transport reduces the dependence of day-night temperature differences upon moisture content [2].

Acknowledgment

The authors wish to thank the reviewers for their helpful comments.

References

[1] J. Hollinger, R. Lo, G. Poe, R. Savage, and J. Pierce, *Special Sensor Microwave/Imager User's Guide*. Washington, DC: Naval Res. Lab., 1987.

[2] Y.-A. Liou and A. W. England, "A land surface process/radiobrightness model with coupled heat and moisture transport in soil," *IEEE Trans. Geosci. Remote Sensing*, to be published.

[3] K. Watson, "Geologic applications of thermal infrared images," *Proc. IEEE*, pp. 370–379, 1975.

[4] A. B. Kahle, "A simple thermal model of the earth's surface for geologic mapping by remote sensing," *J. Geophys. Res.*, vol. 11, pp. 380–387, Apr. 10, 1977.

[5] J. C. Price, "Thermal inertia mapping: A new view of the earth," *J. Geophys. Res.*, vol. 82, pp. 2582–2590, 1977.

[6] ——, "The potential of remotely sensed thermal infrared data to infer surface moisture and evaporation," *Water Resources Res.*, vol. 16, pp. 787–795, 1980.

[7] A. W. England, "Radiobrightness of diurnally heated, freezing soil," *IEEE Trans. Geosci. Remote Sensing*, vol. 28, pp. 464–476, July 1990.

[8] A. W. England, J. F. Galantowicz, and B. W. Zuerndorfer, "A volume scattering explanation for the negative spectral gradient of frozen soil," in *Proc. IGARSS'91 Symp.*, Espoo, Finland, June 3–6, 1991, pp. 1175–1177.

[9] A. W. England, J. F. Galantowicz, and M. S. Schretter, "The radiobrightness thermal inertia measure of soil moisture," *IEEE Trans. Geosci. Remote Sensing*, vol. 30, no. 1, pp. 132–139, Jan. 1992.

[10] Y.-A. Liou and A. W. England, "An annual model of SSM/I radiobrightness for dry soil," in *Proc. IGARSS'92 Symp.*, Houston, TX, May 16–20, 1992.

[11] D. A. de Vries, "Thermal properties of soils," in *Physics of Plant Environment.*, W. R. van Wijk, Ed. Amsterdam, The Netherlands: North-Holland, 1963, pp. 210–235.

[12] P. C. D. Milly and P. S. Eagleson, "The coupled transport of water and heat in a vertical soil column under atmospheric excitation," R. M. Parsons Lab., Dep. Civil Eng., Mass. Inst. Technol., Cambridge, Tech. Rep. 258, 1980.

[13] ——, "Parameterization of moisture and heat fluxes across the land surface for use in atmospheric general circulation models," R. M. Parsons Lab., Dep. Civil Eng., Mass. Inst. Technol., Cambridge, Tech. Rep. 279, 1982.

[14] P. C. D. Milly, "Moisture and heat transport in hysteretic, inhomogeneous porous media: A matric head based formulation and a numerical model," *Water Resource Res.*, vol. 18, pp. 489–498, June 1982.

[15] P. J. Camillo, R. J. Gurney, and T. J. Schmugge, "A soil and atmospheric boundary layer model for evapotranspiration and soil moisture studies," *Water Resource Res.*, vol. 19, pp. 371–380, 1983.

[16] P. C. D. Milly, "A simulation analysis of thermal effects on evaporation from soil," *Water Resource Res.*, vol. 20, pp. 1087–1098, Aug. 1984.

[17] L. B. Bach, "Soil water movement in response to temperature gradients: Experimental measurements and model evaluation," in *Soil Sci. Soc. Amer. Proc.*, 1992, vol. 56, pp. 37–46.

[18] O. B. Andersland, and D. M. Anderson, *Geotechnical Engineering for Cold Regions*. New York: McGraw-Hill, 1978.

[19] C. Rossi and J. R. Nimmo, "Modeling of soil water retention from saturation to oven dryness," *Water Resource Res.*, vol. 30, pp. 701–708, Mar. 1994.
[20] K. E. Trenberth, Ed., *Climate System Modeling*. Cambridge: Cambridge Univ. Press, 1992, pp. 454–457.
[21] J. P. Peixoto and A. H. Oort, *Physics of Climate*. New York: American Inst. Phys., 1992, pp. 235–239.
[22] J. V. Iribarne and W. L. Godson, *Atmospheric Thermodynamics*, 2nd ed. Norwell, MA: Kluwer, 1981.
[23] M. C. Dobson, F. T. Ulaby, M. T. Hallikainen, and M. A. El-Rayes, "Microwave dielectric behavior of wet soil—Part II: Dielectric mixing models," *IEEE Trans. Geosci. Remote Sensing*, vol. GRS-1, pp. 35–46, Jan. 1985.
[24] F. T. Ulaby, R. K. Moore, and A. K. Fung, *Microwave Remote Sensing, Active and Passive*, vol. III. Norwood, MA, 1986.
[25] U. Wegmüller, C. Mätzler, and E. Schanda, "Microwave signatures of bare soil," *Adv. Space Res.*, pp. 307–316, 1989.
[26] J. F. Galantowicz (A. W. England, Principal Investigator), "Field data report for the first radiobrightness energy balance experiment (REBEX-1), Oct. 1992–Apr. 1993, Sioux Falls, South Dakota," UM Radiation Lab., Tech. Rep. RL-913, Feb. 1995.
[27] E. J. Kim (A. W. England, Principal Investigator), "Field data report for the third radiobrightness energy balance experiment (REBEX-3), Sept. 1994–Sept. 1995, wet acidic tundra on the Alaskan North Slope," UM Radiation Lab., Tech. Rep., to be published.

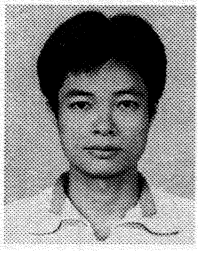

Yuei-An Liou (S'91) received the B.S. degree in electrical engineering from National Sun Yat-Sen University, Kaohsiung, Taiwan, the M.S.E. degree in electrical engineering, and the M.S. degree in atmospheric and space sciences from the University of Michigan, Ann Arbor, in 1987, 1992, and 1994, respectively. He is currently a Ph.D. candidate with the Department of Electrical Engineering and Atmospheric, Oceanic, and Space Sciences at the University of Michigan, Ann Arbor.

From 1989 to 1990, he was a Research Assistant with the National Taiwan University Robotics Laboratory. Since May 1991, he has been a Graduate Research Assistant at the University of Michigan Radiation Laboratory, working in the field of geophysical remote sensing. His interests include energy and moisture transport in subsurface porous media, land-atmosphere interactions, microwave radiometric studies of terrains and atmosphere, and the coupling of these interactions to atmospheric models.

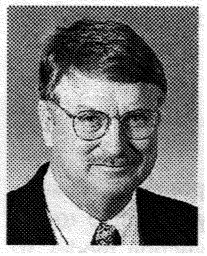

A. W. England (M'87–SM'89–F'95) received the B.S. and M.S. degrees in geology and geophysics (1965) and the Ph.D. degree in geophysics (1970) from the Massachusetts Institute of Technology, Cambridge.

His research interests have included terrestrial heat flow; geomagnetic and gravimetric studies in the Rocky Mountains and in Antarctica; radar studies of temperate and polar glaciers; and microwave studies of snow, ice, freezing soils, and planetary regoliths. His current research concerns the use of sattelite radiobrightness as feedback to temporal models of surface hydrology. He was with the U.S. Geological Survey from 1972 to 1979 where he served as Geophysicist, as Deputy Chief of the Office of Geochemistry and Geophysics, and on several federal committees concerned with technology, Antarctic policy, and nuclear waste containment. He was a NASA Scientist-Astronaut from 1967 to 1972 and Senior Scientist-Astronaut from 1979 to 1988. He was Mission Scientist for Apollo's 13 and 16; flew as a Mission Specialist on Space Shuttle Challenger's Spacelab 2 Mission in 1985—a solar astronomy and plasma physics mission; and was Program Scientist for Space Station during 1986 and 1987. He is a member of the National Research Council's Space Studies Board and chair of their Committee on Research and Analysis. He was an adjunct Professor at Rice University, and is now Professor of Electrical Engineering and Computer Science, Professor of Atmospheric, Oceanic and Space Science, and Associate Dean of the Rackman Graduate School at the University of Michigan. He has served as Associate Editor for the *Journal of Geophysical Research*.

Dr. England is a member of the AGU. He has served on the Administrative Committee of the Geoscience and Remote Sensing Society.